

CREEP, RECOVERY, AND WAVES IN A NONLINEAR FIBER-REINFORCED VISCOELASTIC SOLID*

M. DESTRADE[†] AND G. SACCOMANDI[‡]

Abstract. We present a constitutive model capturing some of the experimentally observed features of soft biological tissues: nonlinear viscoelasticity, nonlinear elastic anisotropy, and nonlinear viscous anisotropy. For this model we derive the equation governing rectilinear shear motion in the plane of the fiber reinforcement; it is a nonlinear partial differential equation for the shear strain. Specializing the equation to the quasi-static processes of creep and recovery, we find that usual (exponential-like) time growth and decay exist in general, but that for certain ranges of values for the material parameters and for the angle between the shearing direction and the fiber direction, some anomalous behaviors emerge. These include persistence of a nonzero strain in the recovery experiment, strain growth in recovery, strain decay in creep, disappearance of the solution after a finite time, and similar odd comportments. For the full dynamical equation of motion, we find kink (traveling wave) solutions which cannot reach their assigned asymptotic limit.

Key words. fiber reinforcement, nonlinear creep and recovery, traveling waves

AMS subject classifications. 74D10, 74A10, 74H05, 74G30

DOI. 10.1137/060664483

1. Introduction. Many biological, composite, and synthetic materials must be modeled as fiber-reinforced nonlinearly elastic solids. Hence, the anisotropy due to the presence of collagen fibers in many biological materials has been studied extensively within the constitutive context of fiber-reinforced materials by several authors (see, for example, Humphrey (2002) and the references therein.) In nonlinear elasticity, the macroscopic response of an anisotropic material is given in terms of a strain-energy function, which itself depends on a set of independent deformation invariants. This formulation captures a great variety of phenomena related to the behavior of fiber-reinforced materials, e.g., the examination of fiber instabilities, using loss of ellipticity (see Merodio and Ogden (2002), (2003), and the references therein).

Generally speaking, a reinforcement is added to a given material with the aim of avoiding a possible failure under operating conditions. Therefore it is important to develop a detailed study showing how to introduce reinforcements into a material in order to control the possible development of a boundary layer structure. Our goal here is to provide a first step in this direction. We make several simplifications and ad hoc assumptions. First, we limit ourselves to the consideration of *only one fiber direction* and second, we consider a *one-dimensional motion* in the bulk of an infinite body. Here the motion is linearly polarized in a direction normal to the plane containing the direction of propagation and the direction of the fibers. We acknowledge that more complex anisotropies, geometries, and couplings arise in biomechanical applications. For instance, the mechanics of the aorta involves two families of parallel fibers, tri-axial motions, and blood flow/arterial wall coupling. However, we argue that some

*Received by the editors July 7, 2006; accepted for publication (in revised form) June 12, 2007; published electronically October 10, 2007. This work was supported by a Fellowship from the City of Paris.

<http://www.siam.org/journals/siap/68-1/66448.html>

[†]Institut Jean Le Rond d'Alembert (UMR 7190), CNRS/Université Pierre et Marie Curie, 4 place Jussieu, case 162, 75252 Paris Cedex 05, France (destrade@lmm.jussieu.fr).

[‡]Dipartimento di Ingegneria Industriale, Università degli Studi di Perugia, 06125 Perugia, Italy (giuseppe.saccomandi@unile.it).

major characteristics of biological soft tissues are encompassed in the choices of transverse isotropy, of infinite extent, and of a motion governed by an ordinary differential equation. Indeed the anisotropy due to the presence of one family of parallel fibers complicates the governing equations to an extent which is only marginally less than that due to the presence of two families of parallel fibers. Also, soft biological tissues are nearly incompressible, and a (compressive) longitudinal wave is difficult to observe; it thus make sense to focus on transverse shear motions, which are useful in imaging technologies. Our third assumption is that the elastic strain energy is the sum of an isotropic part and an anisotropic part (called a *reinforcing model*), in order to model an isotropic base material augmented by a uniaxial reinforcement in the *fiber direction*. Albeit strong, this constitutive assumption is now common and used by many authors (e.g., Triantafyllidis and Abeyaratne (1983), Qiu and Pence (1997), Merodio and Ogden (2002)). Finally, we assume that the solid is viscoelastic, and here we assume not only Newtonian viscosity (proportional to the stretching tensor) but also fiber-oriented (anisotropic) viscosity. That latter assumption is strong but can be removed from our calculations by taking a constant to be zero. We believe that it might be useful in modeling the well-documented physiological effect of stretching training in sport medicine, which is that it affects the viscosity of tendon structures but not their elasticity (Taylor et al. (1990); Kubo, Kanehisa, and Fukunaga (2002)).

We divide the article into the following sections. Section 2 presents the constitutive model and the derivation of the equation governing the rectilinear shear motion. As expected, this equation is nonlinear in the shear strain: it is a second-order partial differential equation, with cubic nonlinearity. To initiate its resolution, we first look at the quasi-static experiment of recovery in section 3. Then we have a first-order ordinary differential equation, and we find that it can lead to unusual behaviors when certain conditions (strong anisotropy, large angle between the shearing direction and the fibers) are met. The same is true of the case of creep, treated in section 4. Basically, it turns out that the nonlinearity introduces ranges of material parameters and angles for which an expected behavior—say, strain growth in creep—can be turned on its head, and lead to strain decay with time in creep, say. In the course of the investigation we develop synthetic tools of analysis which highlight the boundaries of these ranges. They also guide us for the resolution of the full dynamical equation of motion, which we tackle in section 5 for traveling wave solutions. Again the solution may behave in an unexpected way, provided that the anisotropy is strong enough and the fibers are in compression. Finally, section 6 recaps the results and puts them into a wider context.

2. Basic equations.

2.1. The viscoelastic anisotropic model. We describe the motion of a body by a relation $\mathbf{x} = \mathbf{x}(\mathbf{X}, t)$, where \mathbf{x} denotes the current coordinates of a point occupied by the particle of coordinates \mathbf{X} in the reference configuration at the time t .

We introduce $\mathbf{F} = \partial\mathbf{x}/\partial\mathbf{X}$, the deformation gradient, and $\mathbf{C} = \mathbf{F}^T\mathbf{F}$, the right Cauchy–Green strain tensor. We focus on *incompressible materials* for which all admissible deformations must be isochoric, or equivalently, for which the relation $\det \mathbf{F} = 1$ must hold at all times.

The body is reinforced with one family of parallel fibers. Our first assumption is that the unit vector \mathbf{a}_0 , giving the fiber direction in the reference configuration, is independent of \mathbf{X} . The stretch along the fiber direction is $\sqrt{\mathbf{a}_0 \cdot \mathbf{C} \mathbf{a}_0} = \sqrt{\mathbf{a} \cdot \mathbf{a}}$, where $\mathbf{a} = \mathbf{F} \mathbf{a}_0$.

We may now introduce the elastic part of our constitutive model. We consider

the so-called *standard reinforcing model*, which is a quite simple generalization to anisotropy of the neo-Hookean model (Triantafyllidis and Abeyaratne (1983); Qiu and Pence (1997)). For the standard reinforcing model, the strain-energy density is given by

$$(2.1) \quad W = \frac{\mu}{2} [(I_1 - 3) + \gamma_0(I_4 - 1)^2], \quad \text{where } I_1 = \text{tr } \mathbf{C}, \quad I_4 = \mathbf{a}_0 \cdot \mathbf{C} \mathbf{a}_0 = \mathbf{a} \cdot \mathbf{a}.$$

Here $\mu > 0$ is the infinitesimal shear modulus of the isotropic neo-Hookean matrix, $\gamma_0 > 0$ is the *elastic anisotropy parameter*, and the invariant I_4 measures the squared stretch in the fiber direction. Mechanical tests show that the neo-Hookean strain energy function $\mu(I_1 - 3)/2$ fits uniaxial data rather well for arteries (Gundiah, Ratcliffe, and Pruitt (2007)), while the anisotropic term $\gamma_0(I_4 - 1)^2$ is adequate to describe a reinforced material which penalizes deformation in the fiber direction (Merodio and Ogden (2003)).

The spatial velocity gradient $\mathbf{L}(\mathbf{X}, t)$ associated with a motion is defined as $\mathbf{L} = \text{grad } \mathbf{v}$, where $\mathbf{v} = \partial \mathbf{x} / \partial t$ is the velocity, and the stretching tensor \mathbf{D} is defined as $\mathbf{D} = \frac{1}{2}(\mathbf{L} + \mathbf{L}^T)$. For incompressible materials, $\text{tr } \mathbf{D} = 0$ at all times. Newtonian viscous fluids possess a constitutive term in the form $2\nu \mathbf{D}$, where ν is a constant. For our special solid, we modulate the Newtonian viscosity with an anisotropic term, by replacing ν with $\nu[1 + \gamma_1(I_4 - 1)]$, where $\gamma_1 > 0$ is the *viscous anisotropy parameter*. We show in the course of the paper that this simple choice of anisotropic viscosity captures the essential characteristics of attenuation in soft biological fibrous tissues. According to Baldwin et al. (2006), ultrasonic measurements of freshly excised myocardium show that “the attenuation coefficient was found to increase as a function of frequency in an approximately linear manner and to increase monotonically as a function of angle of insonification from a minimum perpendicular to a maximum parallel relative to the direction of the myofibers.”

We are now ready to give the complete Cauchy stress tensor of our viscoelastic, transversally isotropic material as

$$(2.2) \quad \mathbf{T} = -p\mathbf{I} + \mu[\mathbf{B} + \gamma_0(I_4 - 1)\mathbf{a} \otimes \mathbf{a}] + 2\nu[1 + \gamma_1(I_4 - 1)]\mathbf{D},$$

where the p is the yet indeterminate Lagrange multiplier introduced by the incompressibility constraint, and $\mathbf{B} = \mathbf{F}\mathbf{F}^T$ is the left Cauchy–Green tensor.

2.2. Shear motion. We take a fixed orthonormal triad of vectors $(\mathbf{i}, \mathbf{j}, \mathbf{k})$, and call X, Y, Z the reference coordinates; hence $\mathbf{X} = X\mathbf{i} + Y\mathbf{j} + Z\mathbf{k}$. The triad is such that the unit vector in the fiber direction lies in the XY plane; hence,

$$(2.3) \quad \mathbf{a}_0 = \cos \theta \mathbf{i} + \sin \theta \mathbf{j}$$

(say), where $\theta \in [0, \pi]$ is the angle between the X -axis and the fibers.

We then consider the *rectilinear shearing motion*,

$$(2.4) \quad x = X + u(Y, t), \quad y = Y, \quad z = Z,$$

where the antiplane displacement u is real and finite. Then the components of the gradient of deformation \mathbf{F} and of its inverse are given by

$$(2.5) \quad \mathbf{F} = \begin{bmatrix} 1 & U & 0 \\ 0 & 1 & 0 \\ 0 & 0 & 1 \end{bmatrix}, \quad \mathbf{F}^{-1} = \begin{bmatrix} 1 & -U & 0 \\ 0 & 1 & 0 \\ 0 & 0 & 1 \end{bmatrix},$$

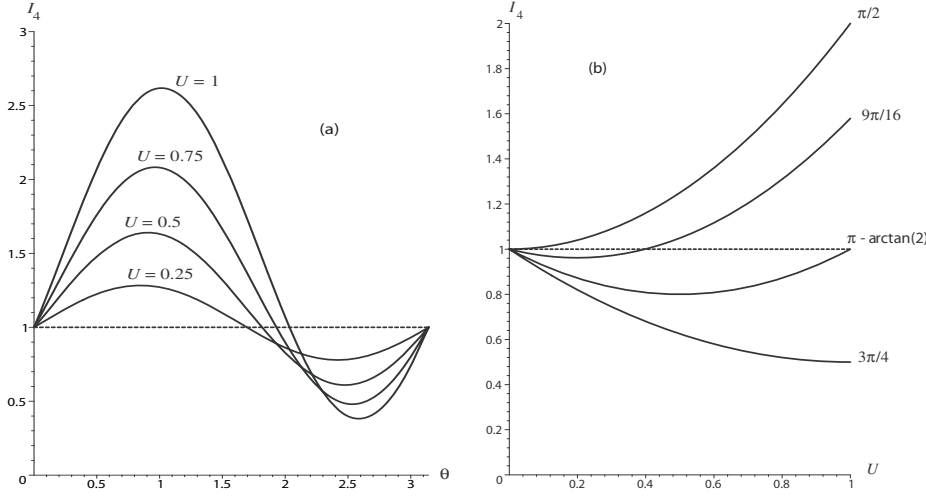


FIG. 2.1. Variations of the squared stretch in the fiber direction: (a) with the angle and (b) with the shear. When $I_4 > 1$, the fibers are in extension; when $I_4 < 1$, they are in compression.

where $U = \partial u / \partial Y$ is the *amount of shear*. The left and right Cauchy–Green tensors are thus

$$(2.6) \quad \mathbf{B} = \begin{bmatrix} U^2 + 1 & U & 0 \\ U & 1 & 0 \\ 0 & 0 & 1 \end{bmatrix}, \quad \mathbf{C} = \begin{bmatrix} 1 & U & 0 \\ U & U^2 + 1 & 0 \\ 0 & 0 & 1 \end{bmatrix},$$

respectively, from which the expressions of the invariants I_1 and I_4 follow,

$$(2.7) \quad I_1 = 3 + U^2, \quad I_4 = 1 + U \sin 2\theta + U^2 \sin^2 \theta.$$

Figure 2.1(a) shows the variations of I_4 with θ for several values of U between 0 and 1. When $I_4 > 1$ the fibers are in extension, and when $I_4 < 1$ they are in compression; the figure shows that this latter behavior occurs in a smaller and smaller angular range, but is more and more pronounced, as the amount of shear is increased. Conversely, Figure 2.1(b) shows the variations of I_4 with U for several values of θ ; when $0 < \theta < \pi/2$, the fibers are always in extension, and when $\pi - \tan^{-1}(2) = 2.034 < \theta < \pi$, they are always in compression for $0 \leq U \leq 1$. We refer to the paper by Qiu and Pence (1997) for similar figures and closely related discussions.

In the deformed configuration, we find that $\mathbf{a} = (\cos \theta + U \sin \theta)\mathbf{i} + \sin \theta \mathbf{j}$. The remaining tensors required to compute the Cauchy stress tensor (2.2) are

$$(2.8) \quad \mathbf{a} \otimes \mathbf{a} = \begin{bmatrix} (\cos \theta + U \sin \theta)^2 & (\cos \theta + U \sin \theta) \sin \theta & 0 \\ (\cos \theta + U \sin \theta) \sin \theta & \sin^2 \theta & 0 \\ 0 & 0 & 0 \end{bmatrix}$$

and

$$(2.9) \quad \mathbf{D} = \frac{1}{2} \begin{bmatrix} 0 & U_t & 0 \\ U_t & 0 & 0 \\ 0 & 0 & 0 \end{bmatrix},$$

so that the nonzero components of \mathbf{T} are $T_{33} = -p + \mu$ and

$$(2.10) \quad \begin{aligned} T_{11} &= -p + \mu(1 + U^2) + \mu\gamma_0(I_4 - 1)(\cos\theta + U \sin\theta)^2, \\ T_{22} &= -p + \mu + \mu\gamma_0(I_4 - 1)\sin^2\theta, \\ T_{12} &= \mu U + \mu\gamma_0(I_4 - 1)(\cos\theta + U \sin\theta)\sin\theta + \nu[1 + \gamma_1(I_4 - 1)]U_t. \end{aligned}$$

Now the equations of motion $\operatorname{div} \mathbf{T} = \rho \mathbf{x}_{tt}$ reduce to the two scalar equations $-p_x + T_{12,y} = \rho u_{tt}$ and $-p_y + T_{22,y} = \rho u_{tt}$. Differentiating the former with respect to y and the latter with respect to x , and eliminating p_{xy} , we arrive at a single governing equation for the rectilinear shear motion:

$$(2.11) \quad \begin{aligned} \rho U_{tt} &= \mu U_{yy} + \mu\gamma_0 \sin^2\theta [U(2\cos\theta + U \sin\theta)(\cos\theta + U \sin\theta)]_{yy} \\ &\quad + \nu U_{tyy} + \nu\gamma_1 \sin\theta [UU_t(2\cos\theta + U \sin\theta)]_{yy}. \end{aligned}$$

Using the scalings $\tilde{t} = \mu t/\nu$ and $\tilde{y} = y/L$ (where L is a characteristic length to be specified later on a case-by-case basis), we write this equation in dimensionless form as

$$(2.12) \quad \begin{aligned} \varepsilon U_{\tilde{t}\tilde{t}} &= U_{\tilde{y}\tilde{y}} + \gamma_0 \sin^2\theta [U(2\cos\theta + U \sin\theta)(\cos\theta + U \sin\theta)]_{\tilde{y}\tilde{y}} \\ &\quad + U_{\tilde{t}\tilde{y}\tilde{y}} + \gamma_1 \sin\theta [UU_t(2\cos\theta + U \sin\theta)]_{\tilde{y}\tilde{y}}, \end{aligned}$$

where $\varepsilon = \rho\mu L^2/\nu^2$. This is the main equation of our study. For convenience we drop the tildes in the remainder of the paper. We also introduce the functions

$$(2.13) \quad \begin{aligned} f(\gamma_0, U, \theta) &= 1 + \gamma_0 \sin^2\theta(2\cos\theta + U \sin\theta)(\cos\theta + U \sin\theta), \\ g(\gamma_1, U, \theta) &= 1 + \gamma_1 U \sin\theta(2\cos\theta + U \sin\theta), \end{aligned}$$

so that (2.13) is now

$$(2.14) \quad \varepsilon U_{tt} = [Uf(\gamma_0, U, \theta) + U_t g(\gamma_1, U, \theta)]_{yy}.$$

3. Nonlinear anisotropic recovery. Our first investigation is placed in the quasi-static approximation, where we study the influence of elastic anisotropy and viscous anisotropy on the classic experiment of viscous *recovery*. We imagine that the material is sheared and that at $t = 0$ the shear stress is removed: $T_{12}(0) = 0$. Here the characteristic length L is the displacement at $t = 0$ from which the material will relax to the unstressed state.

In the quasi-static case, we neglect the inertia term of (2.13) and may thus integrate it twice to give the following first-order ordinary differential equation:

$$(3.1) \quad Uf(\gamma_0, U, \theta) + U_t g(\gamma_1, U, \theta) = 0.$$

Here we take the constants of integration to be zero, according to the context of recovery, as explained above. We then solve the equation as

$$(3.2) \quad \int \frac{g(\gamma_1, U, \theta)}{Uf(\gamma_0, U, \theta)} dU = -t + \text{const.},$$

where the constant is computed so that $U(0) = 1$.

When $\theta = 0$, the fibers are not active with respect to the deformation, and we recover the classical result of isotropic viscoelastic recovery: $U(t) = e^{-t}$.

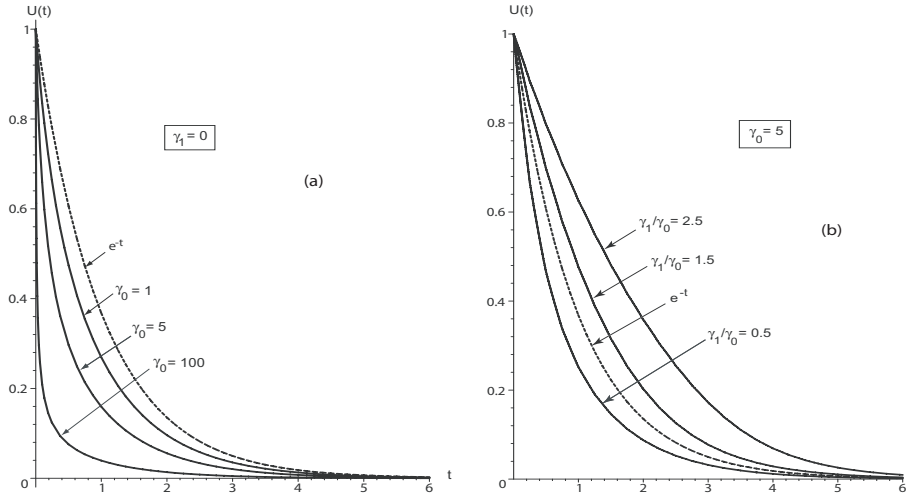


FIG. 3.1. Time recovery function when $\theta = \pi/2$: (a) $\gamma_1 = 0$ and $\gamma_0 = 1, 5, 100$; (b) $\gamma_0 = 5$ and $\gamma_1 = 0.5, 1.5, 2.5$. The recovery function for an isotropic solid is also plotted (dotted curve).

When $\theta = \pi/2$, the anisotropic effects are at their strongest. In that case the integral above has a compact expression, and we find

$$(3.3) \quad U \left[\frac{1 + \gamma_0 U^2}{1 + \gamma_0} \right]^{\frac{1}{2} \left(\frac{\gamma_1}{\gamma_0} - 1 \right)} = e^{-t}.$$

We now take $\gamma_1 = 0$ (no anisotropic viscosity) and $\gamma_0 = 1, 5, 100$ (recall that the fibers are inextensible in the limit $\gamma_0 \rightarrow \infty$). Figure 3.1(a) shows that as the anisotropic effect becomes more pronounced, the recovery is quicker; in other words, the influence of elasticity becomes stronger as γ_0 increases. Then we fix γ_0 at 5, for instance, and look at the role played by the anisotropic viscosity, by taking in turn $\gamma_1/\gamma_0 = 0.5, 1.5, 2.5$. We find in Figure 3.1(b) that, as expected, the viscous recovery is slower as γ_1 increases.

When $\theta \neq 0, \theta \neq \pi/2$, other behaviors arise, which call for a detailed analysis. In particular, the exponential, or near-exponential, decay toward zero as $t \rightarrow \infty$ is not necessarily ensured, especially when the anisotropic effects are strong and the fibers are oriented at a large angle $\theta > \pi/2$. Clearly, $U_t = 0$ when $f = 0$, according to (3.2). Also, $U_t < 0$ when f and g are of the same sign, and $U_t > 0$ when f and g are of opposite signs. These two functions are quadratic in U . If they have no real roots in U , then they are both of the positive sign and $U_t < 0$. (This is clearly the case in the region $0 < \theta < \pi/2$.) If they have real roots, then they may change sign, and U might be an *increasing* function of t . This happens for f and for g when $\pi/2 < \theta < \pi$ and

$$(3.4) \quad \gamma_0 \geq \frac{4}{\cos^2 \theta \sin^2 \theta}, \quad \gamma_1 \geq \frac{1}{\cos^2 \theta},$$

respectively. In Figure 3.2, the region C corresponds to the first inequality, where the delimiting curve has a vertical asymptote at $\theta = \pi/2$, a vertical asymptote at $\theta = \pi$, and a minimum at $\theta = \pi/4, \gamma_0 = 16$; we recall that Qiu and Pence (1997) showed that

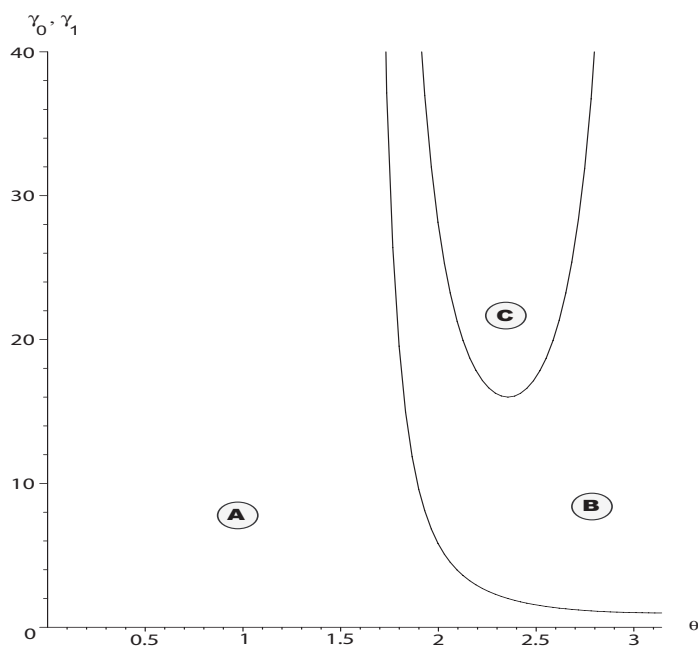


FIG. 3.2. Recovery: regions where the sign of U_t may change.

when $\gamma_0 > 16$, “simple shear at certain fiber orientations involves negative shear stress in the shearing direction for certain positive shears.” The region B corresponds to the second inequality, where the delimiting curve has a vertical asymptote at $\theta = \pi/2$ and an horizontal asymptote at $\gamma_1 = 1$. In the region A, neither inequality is satisfied.

3.1. Weak anisotropy. First, we take both γ_0 and γ_1 in region A. This is the simplest case because f and g are then both positive, and so U_t is always negative (damped recovery). We took several representative examples in this region (say, $\theta = \pi/4$, $\gamma_0 = 20$, $\gamma_1 = 1$) and checked, through integration and implicit plotting, that the graphs are indeed of the same nature as those in Figure 3.1.

3.2. Strong elastic anisotropy. Second, we take γ_1 in region A, by fixing it at $\gamma_1 = 1$, say. In that region, $g > 0$ always, and thus the sign of U_t is the opposite of the sign of f . Then we take $\gamma_0 = 20$, which is above the minimum of region C. In Figure 3.3, we plot the locus for the values of U as functions of θ such that $f(20, U, \theta) = 0$. Outside the resulting oval shape, $f > 0$, and inside, $f < 0$. We also plotted the line $U = 1$, which intersects the oval at $\theta_{\min} = 2.136$ and $\theta_{\max} = 2.221$. Recall that $U(0) = 1$.

When $\theta > \theta_{\max}$, $U(t)$ starts at 1 and decreases because $f > 0$ so that $U_t < 0$; as U decreases toward 0, U_t tends to zero according to $(3.2)_1$, but takes an infinite time to do so, according to $(3.2)_2$; hence $U = 0$ is a horizontal asymptote and the recovery is “classical”; see plot (i) in Figure 3.3, traced at $\theta = 2.4$ (notice, however, that the recovery is not exponential because the second derivative of U clearly changes sign as t increases, in contrast with e^{-t} , traced in dotted lines).

When $\theta_{\min} < \theta < \theta_{\max}$, $U(t)$ starts at 1 and then grows until it hits the upper side of the oval, taking an infinite time to do so; then this upper bound gives a horizontal asymptotic value, *above the initial value* (see plot (ii) in Figure 3.3), traced at $\theta = 2.2$.

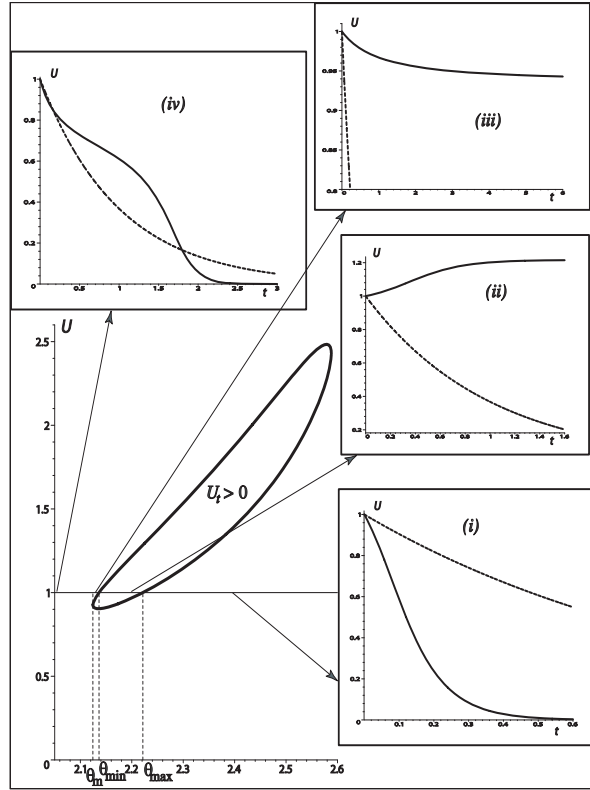


FIG. 3.3. Types of time recovery functions for $\gamma_0 = 20$, $\gamma_1 = 1$ (strong elastic anisotropy). The amount of shear U starts at 1 for $t = 0$. Outside the oval shape, $U_t < 0$ and U decreases as in (i) and (iv): decay toward zero; and in (iii): decay toward a value > 0 . Inside the oval shape, $U_t > 0$ and U increases as in (ii): growth toward a value > 1 . The recovery function e^{-t} for an isotropic solid is also plotted (dotted curves).

When $\theta_m < \theta < \theta_{\min}$, where $\theta_m = 2.124$ is the angle at which the oval plot has a vertical tangent, $U(t)$ starts at 1 and then decreases until it hits the upper side of the oval, below 1 but above 0; then this lower bound gives a horizontal asymptotic value, above zero (see plot (iii) in Figure 3.3), traced at $\theta = 2.125$.

Finally, when $\theta < \theta_m$, $U(t)$ starts at 1 and then decreases until zero; then this lower bound gives zero as a horizontal asymptotic value (see plot (iv) in Figure 3.3), traced at $\theta = 2.05$. Notice that the second derivative changes signs three times as t increases.

3.3. Strong viscous anisotropy. Third, we take γ_0 outside the C region, by fixing it at $\gamma_0 = 1$, say. In that region, $f > 0$ always, and thus the sign of U_t is the opposite of the sign of g . Then we allow γ_1 to be in region B, and thus allow g (and U_t) to change sign with increasing θ , by taking $\gamma_1 = 3.0$, say. In Figure 3.4, we plotted the values of U as functions of θ such that $g(3, U, \theta) = 0$ and obtained the thick-line shape. Outside the shape, $g > 0$, and inside, $g < 0$. We also plotted the horizontal line $U = 1$, which intersects the shape at $\theta_{\min} = 2.356$ and $\theta_{\max} = 2.820$, and the vertical line $\theta = \theta_m = 2.186$, which is tangent to the shape.

Now when $\theta < \theta_m$ or $\theta > \theta_{\max}$, $U(t)$ starts at 1 and decreases until zero; as $U \rightarrow 0$, the denominator in the integral tends to zero, indicating that it takes an

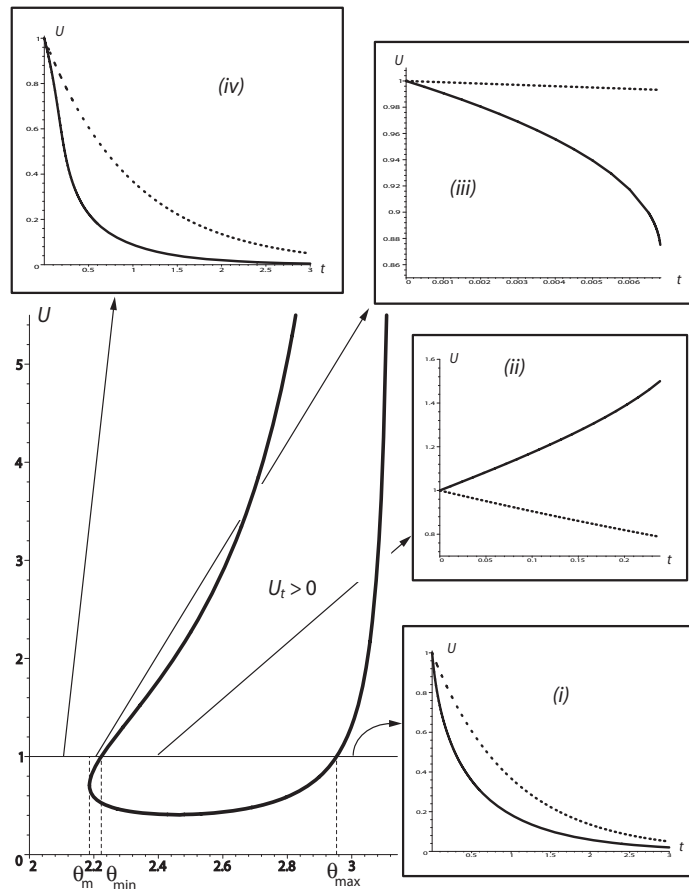


FIG. 3.4. Types of time recovery functions for $\gamma_0 = 1$, $\gamma_1 = 2$ (strong viscous anisotropy). The amount of shear U starts at 1 for $t = 0$. Outside the thick-line shape, $U_t < 0$ and U decreases toward zero as in (i) and (iv). Inside the thick-line shape, $U_t > 0$ and U increases rapidly as in (ii), until it ceases to exist. There is also an angular region $\theta_m < \theta < \theta_{\min}$ where U decreases rapidly until it ceases to exist; see (iii). The recovery function e^{-t} for an isotropic solid is also plotted (dotted curves).

infinite time to do so; hence, zero is a horizontal asymptote in these cases. To draw Figure 3.4(i) we took $\theta = 3.0$, and for Figure 3.4(iv) we took $\theta = 2.1$; both graphs show a somewhat classical decay with time.

However, when $\theta_{\min} < \theta < \theta_{\max}$, $U(t)$ starts at 1 and then *grows* because $U_t > 0$ inside the thick line shape. Eventually U hits the upper face of the shape, where $g = 0$; then by (3.1), either $Uf = 0$ or $U_t \rightarrow \infty$. Clearly, the first possibility is excluded because $U \neq 0$ when it is larger than 1, and $f \neq 0$ when γ_0 is outside the C region. It follows that U grows and hits the upper face of the shape with a vertical asymptote after a finite time (and then stops because it cannot increase further since $U_t < 0$ outside the shape, it cannot remain constant since $U_t \neq 0$ on the shape, and it cannot decrease since $U_t > 0$ inside the shape). Figure 3.4(ii) shows such behavior for $U(t)$, traced at $\theta = 2.4$.

Finally, when $\theta_m < \theta < \theta_{\min}$, $U(t)$ decays from 1 until it hits the shape from above after a finite time; see Figure 3.4(iii), traced at $\theta = 2.2$. Notice how quickly the final value is reached, compared to the isotropic exponential recovery.

3.4. Strong elastic and viscous anisotropies. In the case where both γ_0 and γ_1 are in the region C, any combination and overlaps of the thick curves presented in Figures 3.3 and 3.4 may arise. The tools presented in the two previous subsections are easily transposed to those possibilities. A special situation arises when the locus of $f = 0$ intersects the locus of $g = 0$; then, the numerator and the denominator in (3.2) may have a common factor so that the integrand simplifies and a regular behavior may appear. This situation is, however, too special to warrant further investigation, and we do not pursue this line of enquiry.

4. Nonlinear anisotropic creep. Our second investigation is again placed in the quasi-static approximation, where we now study the influence of elastic anisotropy and viscous anisotropy on the classic experiment of viscous *creep*. As the resulting analysis is similar to that conducted for recovery, we simply outline the main results.

We imagine that the material is sheared and that the shear stress is maintained: $T_{12}(\infty) \neq 0$. Here the characteristic length L is an asymptotic value of the displacement. We neglect the inertial term of (2.13) and integrate it twice to give the ordinary differential equation

$$(4.1) \quad Uf(\gamma_0, U, \theta) + U_t g(\gamma_1, U, \theta) = \text{const.},$$

where we took the constant of the first integration to be zero and the constant of the second integration to correspond to the applied (constant) shear stress, as is usual in the creep problem. More specifically, this constant is taken so that $U(\infty) = 1$, and so is equal to $f(\gamma_0, 1, \theta)$; it follows that the equation above can be written as

$$(4.2) \quad h(\gamma_0, U, \theta)(U - 1) + g(\gamma_1, U, \theta)U_t = 0,$$

where h is defined by

$$(4.3) \quad \begin{aligned} h(\gamma_0, U, \theta) &= [Uf(\gamma_0, U, \theta) - f(\gamma_0, 1, \theta)]/(U - 1) \\ &= 1 + \gamma_0 \sin^2 \theta [1 + \cos^2 \theta + (U + 1) \sin \theta (U \sin \theta + 3 \cos \theta)]. \end{aligned}$$

We then solve the equation as

$$(4.4) \quad \int \frac{g(\gamma_1, U, \theta)}{(U - 1)h(\gamma_0, U, \theta)} dU = -t + \text{const.},$$

where the constant is computed so that $U(0) = 0$. Hence the equations governing creep are almost identical to those governing recovery, with the difference that f is now replaced by h .

Here we are mostly concerned with the question of how, if at all, a state of shear can be reached such that, once removed, the unusual recovery behaviors of the previous section emerge. Thus we concentrate on strong anisotropic effects, with emphasis on strong elastic anisotropy (where the new function h is involved). We traced the regions where g and h , and thus U_t , may change signs and found that the resulting graph is similar to that of Figure 3.2, with the main difference that the minimum of region C is now located at $\theta = 3\pi/4$ and $\gamma_0 = 4$. Thus unusual behavior in creep may occur at much lower levels of elastic anisotropy than in recovery (where the minimum is at $\gamma_0 = 16$). We recall that Qiu and Pence (1997) showed that when $\gamma_0 > 4$, “simple shear at certain fiber orientations involves a nonmonotonic relation between the shear stress in the shearing direction and the amount of shear.”

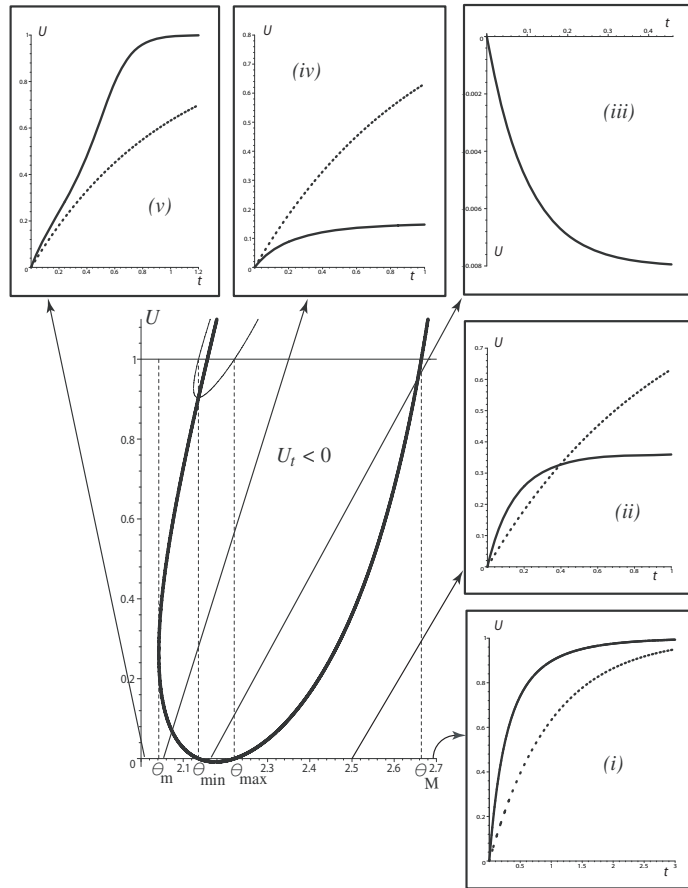


FIG. 4.1. Types of time creep functions for $\gamma_0 = 20$, $\gamma_1 = 1$ (strong elastic anisotropy). The amount of shear U starts at 0 for $t = 0$. Outside the thick-line shape, $U_t > 0$ and U increases as in (i) and (v): growth toward 1, and as in (ii) and (iv): growth toward a value below 1. Inside the thick-line shape, U decreases as in (iii): decay toward a negative value. The creep function $1 - e^{-t}$ for an isotropic solid is also plotted (dotted curves).

4.1. Strong elastic anisotropy. We begin with the case where h plays a major role, that is, when γ_0 is greater than 4. For the purpose of direct comparison with the recovery problem, we take $\gamma_0 = 20$ and $\gamma_1 = 1$, as in section 3.2. Figure 4.1 displays the curve where $h(20, U, \theta) = 0$. Outside the thick-line curve, $U_t > 0$, and inside, $U_t < 0$. The curve intersects the line $U = 0$ twice, at $\theta_{\min} = 2.136$ and at $\theta_{\max} = 2.221$. These are the values at which $f = 0$ intersects $U = 1$ in section 3.2 (see the thin-line shape), because by (4.3), $h(20, 0, \theta_{\min}) = f(20, 1, \theta_{\min}) = 0$ and similarly $h(20, 0, \theta_{\max}) = f(20, 1, \theta_{\max}) = 0$. We also display the vertical lines $\theta = \theta_M = 2.664$, where $h = 0$ intersects $U = 1$, and $\theta = \theta_m = 2.042$, where $h = 0$ has a vertical tangent. Recall that for creep, $U(0) = 0$.

When $\theta > \theta_M$, $U(t)$ starts at 0 and grows toward 1; then U_t tends to zero according to (4.2) but takes an infinite time to do so; hence $U = 1$ is a horizontal asymptote and the creep is “classical.” See plot (i) in Figure 4.1, traced at $\theta = 2.7$ (the exponential creep function of isotropic visco-elasticity ($1 - e^{-t}$) is shown by the dotted line).

When $\theta_{\max} < \theta < \theta_M$ or when $\theta_m < \theta < \theta_{\min}$, $U(t)$ starts at 0 and then grows

until it hits the oval shape, taking an infinite time to do so; then this upper bound gives a horizontal asymptotic value, *below* 1; see plot (ii) in Figure 4.1, traced at $\theta = 2.5$, and plot (iv), traced at $\theta = 2.05$.

When $\theta_{\min} < \theta < \theta_{\max}$, $U(t)$ starts at 0 inside the oval shape, and thus it *decreases* until it hits the lower side of the shape, taking an infinite time to do so; then this lower bound gives a horizontal asymptotic value, *below* 0; see plot (iii) in Figure 4.1, traced at $\theta = 2.17$.

Finally, when $\theta < \theta_m$, $U(t)$ can again grow toward 1; see plot (v) in Figure 4.1, traced at $\theta = 2.0$. Notice, however, that the concavity of the curve changes as t increases.

4.2. Strong viscous anisotropy. Here we remark that the function governing the strength of the viscous anisotropy, namely g , is the same for creep as it is for recovery. Thus, the region where U_t might change sign because of strong viscous anisotropy is the region B of Figure 3.1. Also, the locus of points where $g = 0$ is typically displayed by the thick-line shape of Figure 3.4, and because $g(\gamma_1, 0, \theta) = 1 > 0$ always, this curve never crosses the abscissa $U = 0$. It follows that there is only one situation where viscous anisotropy leads to anomalous creep, when $\theta_{\min} < \theta < \theta_{\max}$; then $U(t)$ starts at zero and grows toward the thick-line shape, which it reaches after a finite time with a vertical asymptote.

4.3. Prestretch and nonlinear anisotropic creep. Here we show how anomalous creep can be avoided (amplified) by stretching (compressing) the solid prior to the shear. Hence, instead of (2.4), we consider the motion

$$(4.5) \quad x = \lambda^{-\frac{1}{2}} X + \lambda u(Y, t), \quad y = \lambda Y, \quad z = \lambda^{-\frac{1}{2}} Z.$$

The following decomposition of the associated deformation gradient shows that the solid is stretched by a ratio λ in the Y direction:

$$(4.6) \quad \mathbf{F} = \mathbf{F}_2 \mathbf{F}_1, \quad \text{where} \quad \mathbf{F}_2 = \begin{bmatrix} 1 & U & 0 \\ 0 & 1 & 0 \\ 0 & 0 & 1 \end{bmatrix}, \quad \mathbf{F}_1 = \begin{bmatrix} \lambda^{-\frac{1}{2}} & 0 & 0 \\ 0 & \lambda & 0 \\ 0 & 0 & \lambda^{-\frac{1}{2}} \end{bmatrix}.$$

(Note that $\mathbf{F}_2 \mathbf{F}_1 \neq \mathbf{F}_1 \mathbf{F}_2$.) The kinematic quantities of section 2.2 are modified accordingly. In particular,

$$(4.7) \quad I_4 = \lambda^{-1} \cos^2 \theta + \lambda^2 \sin^2 \theta + U \lambda^{\frac{1}{2}} \sin 2\theta + U^2 \lambda^2 \sin^2 \theta.$$

The end result is that the differential equation governing creep is changed from (4.2) to

$$(4.8) \quad h^\lambda(\gamma_0, U, \theta)(U - 1) + g^\lambda(\gamma_1, U, \theta)U_t = 0,$$

where h^λ and g^λ are defined by

$$(4.9) \quad h^\lambda(\gamma_0, U, \theta) = \lambda^2 \{ 1 + \gamma_0 \sin^2 \theta [2\lambda^2 \sin^2 \theta + 3\lambda^{-1} \cos^2 \theta - 1 + (U + 1) \sin \theta (U \sin \theta + 3 \cos \theta)] \},$$

$$g^\lambda(\gamma_1, U, \theta) = 1 + \gamma_1 (\lambda^{-1} \cos^2 \theta + \lambda^2 \sin^2 \theta - 1 + U \lambda^{\frac{1}{2}} \sin 2\theta + U^2 \lambda^2 \sin^2 \theta).$$

Figure 4.2 shows the loci of $h^\lambda = 0$ in the case of a strong elastic anisotropy ($\gamma_0 = 30$,

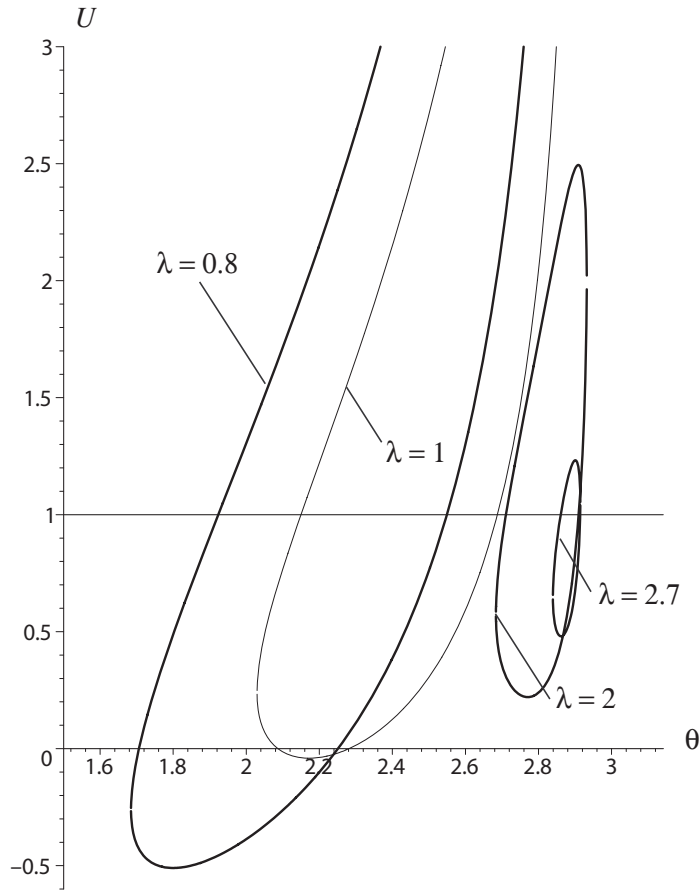


FIG. 4.2. Effect of prestretch on time creep functions for $\gamma_0 = 30$, $\gamma_1 = 1$ (strong elastic anisotropy). The amount of shear U starts at 0 for $t = 0$. Inside the thick-line shapes, U decreases; this situation may arise when the solid is not prestretched ($\lambda = 1$) or when it is compressed ($\lambda = 0.8$). Outside the thick-line shapes, $U_t > 0$ and U increases; this situation may arise when the solid is in extension ($\lambda = 2$, $\lambda = 2.7$).

$\gamma_1 = 1$), for several values of λ . The figure clearly shows that the prestretch λ can be used to control the shape of these curves: if the solid is put in compression first, and sheared for creep next, then the region of potential anomalous creep is increased; if it is put under tension, then the area of the region rapidly decreases and eventually disappears altogether.

5. Nonlinear traveling waves. So far we have looked at how the presence of elastic and viscous fibers affects some quasi-static processes. Typically, creep and recovery connect one state of constant shear (initial) to another (final). Now we examine another class of solutions connecting two constant states of shear, this time *dynamically*, by looking for traveling wave (kink) solutions.

The mathematical theory of one-dimensional transverse traveling waves in isotropic viscoelastic materials with a Kelvin–Voigt type of constitutive equation is well grounded; see, for example, Nishihara (1995) for a clear and complete mathematical approach, or Jordan and Puri (2005) for a specific and explicit example. A traveling

wave is a solution to the equations of motion in the form

$$(5.1) \quad U(Y, t) = U(\xi), \quad \xi = Y - ct,$$

where c is the constant speed; also, U is such that

$$(5.2) \quad \lim_{\xi \rightarrow -\infty} U(\xi) = U_L, \quad \lim_{\xi \rightarrow \infty} U(\xi) = U_R,$$

where U_L and U_R are distinct constants. In what follows, we focus on the case where $U_L = 0$, $U_R = 1$. This case is general up to a rigid translation. Here we take the displacement corresponding to U_R as the characteristic length L .

Substituting (5.1) into (3.2), we obtain

$$(5.3) \quad \varepsilon c^2 U'' = (Uf - cU'g)' ,$$

and then by integration,

$$(5.4) \quad cU'g = (f - \varepsilon c^2)U + \text{const.}$$

By the requirement $U_L = 0$, the constant must be zero. By the requirement $U_R = 1$, we have

$$(5.5) \quad f(\gamma_0, 1, \theta) = \varepsilon c^2.$$

This equation prompts three remarks.

First, we must ensure that $f(\gamma_0, 1, \theta) > 0$. Recall that, according to (2.13),

$$(5.6) \quad f(\gamma_0, 1, \theta) = 1 + \gamma_0 \sin^2 \theta (2 \cos \theta + \sin \theta) (\cos \theta + \sin \theta),$$

and so

$$(5.7) \quad \partial f(\gamma_0, 1, \theta) / \partial \theta = \gamma_0 \sin \theta (4 \cos^3 \theta + 9 \sin \theta \cos^2 \theta - 3 \sin^3 \theta).$$

In Figure 5.1(a) we plot the variations of $[f(\gamma_0, 1, \theta) - 1] / \gamma_0$ with θ , as well as those of its derivative with respect to θ (scaled to $1/8$). Clearly, the function (5.6), viewed as a function of θ , has an absolute minimum and an absolute maximum. The minimum is at $\hat{\theta}$, say, such that $\tan \hat{\theta}$ is that root of the cubic $4 + 9x - 3x^3 = 0$ corresponding to $\pi/2 < \hat{\theta} < \pi$; numerically, $\hat{\theta} = 2.1777$. Then, solving $f(\gamma_0, 1, \hat{\theta}) = 0$ for γ_0 , we find that $f(\gamma_0, 1, \theta) > 0$ when $0 < \gamma_0 < \hat{\gamma}_0 = 18.490$; and that when $\gamma_0 > \hat{\gamma}_0$, there appears a range for θ where $f(\gamma_0, 1, \theta) > 0$ is not insured. Placing ourselves outside that possibility, we deduce from (5.5) that, for a given γ_0 and a given θ , the wave travels with speed

$$(5.8) \quad c = \pm \sqrt{f(\gamma_0, 1, \theta) / \varepsilon}.$$

This is of course expressed in the dimensionless variables of length/ L and time $\times \mu / \nu$. Turning back, if required, to physical variables, we would find that the wave travels with the dimensional speed $\sqrt{\mu f(\gamma_0, 1, \theta) / \nu}$.

The second remark is that, according to (5.5) and (5.6), the wave (when it exists) travels with maximum speed at the angle $\tilde{\theta}$, say, such that $\tan \tilde{\theta}$ is that root of the cubic $4 + 9x - 3x^3 = 0$ corresponding to $0 < \tilde{\theta} < \pi/2$; numerically, $\tilde{\theta} = 1.0910$. Hence the directions of extremal speeds of propagation are always the same, whatever the values of the constitutive parameters μ , γ_0 , and γ_1 . This observation indicates the way for

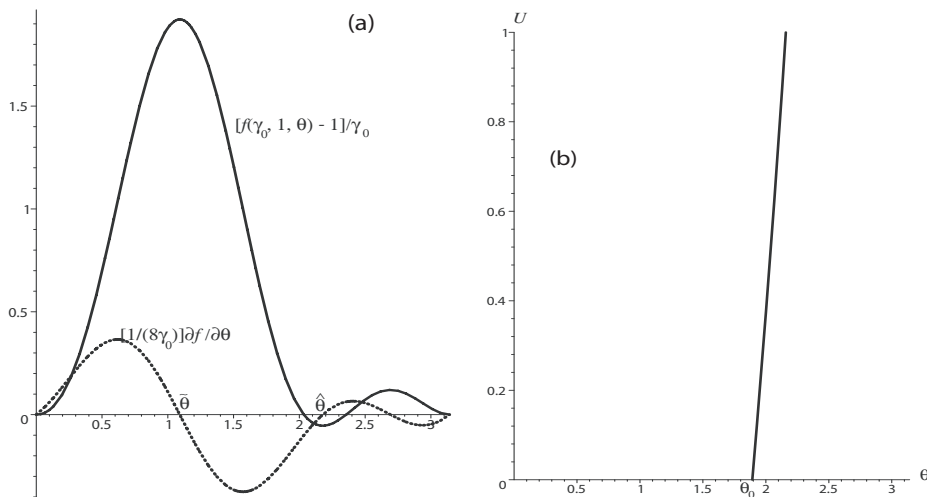


FIG. 5.1. (a) Variations with θ of $[f(\gamma_0, 1, \theta) - 1]/\gamma_0$ and of its derivative, showing an absolute minimum at $\hat{\theta} = 2.1777$. (b) Variations of $-3/\tan\theta - 1$ with θ , crossing the abscissa line at $\theta_0 = 1.8926$.

an acoustic determination of the fiber orientation: if an experimental measurement of the shear wave speed can be made in every direction of a fiber-reinforced viscoelastic nonlinear material, then the fibers are at an angle $\hat{\theta}$ from the direction of the slowest wave and at an angle $\tilde{\theta}$ from the direction of the fastest wave. We recall that for waves in an *isotropic* deformed neo-Hookean material, Ericksen (1953) found that the fastest waves propagate along the direction of greatest initial stretch.

The third remark is that when (5.5) holds,

$$(5.9) \quad f(\gamma_0, U, \theta) - \varepsilon c^2 = \gamma_0 U(U - 1) \sin^3 \theta [U \sin \theta + 3 \cos \theta + \sin \theta].$$

Then the separation of variables, followed by integration of the first-order differential equation (5.4), leads to

$$(5.10) \quad \int \frac{g(\gamma_1, U, \theta)}{U(U - 1) \sin^3 \theta [U \sin \theta + 3 \cos \theta + \sin \theta]} dU = \frac{\gamma_0}{c} \xi + \text{const.},$$

where the constant of integration is arbitrary; without loss of generality, we take it to be such that $U(0) = 1/2$.

Clearly, critical issues arise when either the numerator or the denominator change signs (because then U' changes sign, and it might not be possible to find a solution satisfying the requirements (5.2)). We may take care of the numerator's sign by considering only elastic anisotropy ($\gamma_0 \neq 0$) and discarding viscous anisotropy ($\gamma_1 = 0$); then $g = 1$. For the denominator, however, we note that $U \sin \theta + 3 \cos \theta + \sin \theta$ can change sign for certain ranges of U and θ . Figure 5.1(b) shows the curve $U = -3/\tan \theta - 1$; on its left side, the denominator is positive; on its right side, it is negative. Accordingly, the wave connects 0 to 1 (see Figure 5.2(a)) or is unable to do so (see Figure 5.2(b)). In that latter case, the wave front grows toward an asymptotic value which is less than 1; a second solution exists (dotted curve) with 1 as an asymptotic value, but in the $\xi \rightarrow -\infty$ direction.

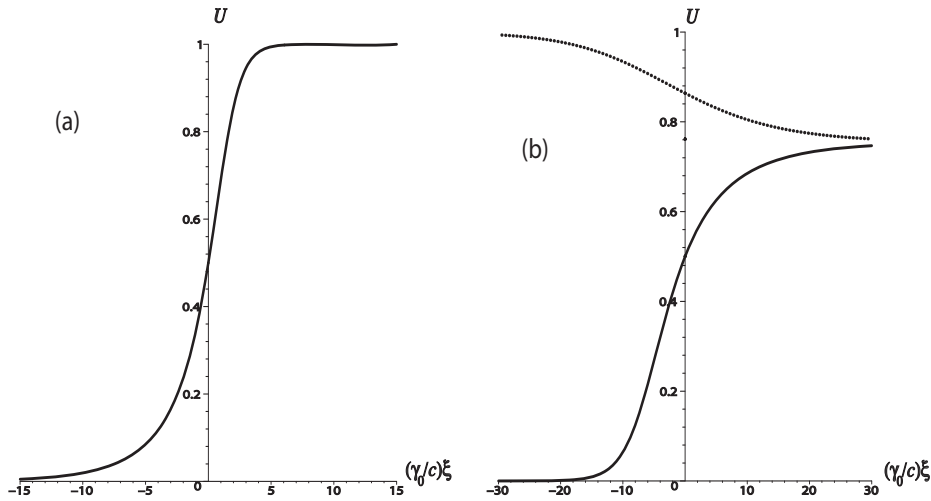


FIG. 5.2. *Traveling wave solution for anisotropic elasticity* ($\gamma_1 = 0$): (a) at $\theta = 1.8$, (b) at $\theta = 2.1$.

As a final remark, we note that when γ_1 is large enough to allow for the possibility that $g = 0$ (strong viscous anisotropy), then a “singular barrier” arises; see Pettet, McElwain, and Norbury (2000).

6. Discussion. In the course of this investigation on nonlinear anisotropic creep, recovery, and waves for fiber-reinforced nonlinear elastic materials, we unearthed some complex mechanical responses. For some range of the constitutive parameters and for some angle ranges of the fiber arrangement, we saw that unusual and possibly aberrant behaviors can emerge.

From a mathematical point of view, we gave a detailed explanation of the reasons for these behaviors, by linking them to the singularities of the determining equations for the amount of shear.

From the mechanical point of view, we pointed out that nonstandard behaviors always occur when the angle between the fiber family and the direction of shear is such that the fibers are compressed; see Figure 2.1. It has been widely demonstrated that several types of instabilities may develop in the case of fiber contraction; see the detailed studies by Triantafyllidis and Abeyaratne (1983), Qiu and Pence (1997), Merodio and Ogden (2002), (2003), (2005a), (2005b), or Fu and Freidin (2004). For example, Merodio, Saccomandi, and Sgura (2007) recently investigated a nonhomogeneous rectilinear shear static deformation for the standard reinforcing model (2.1) and found nonregular solutions (that is, deformations characterized by a discontinuous amount of shear) in fiber-contracted materials.

From a numerical point of view, we recall that a simple model, together with a simple class of solutions, allows a step-by-step control of the simulations. It would indeed be hard to detect nonstandard behaviors by relying solely on a complex numerical finite element method (omitting to conduct a simple analytical methodology such as the one presented in this paper). For example, Holzapfel and Gasser (2001) present a detailed computational study of some viscoelastic fiber-reinforced nonlinear materials, but use values for the material parameters and for the angles which place their simulations outside the problematic ranges. Other studies are placed in the framework of

linear models (even for polymeric materials; see Liu, Kasyanov, and Schoephoerster (2007)), which fail to capture nonstandard behaviors.

From an experimental point of view, our results suggest some simple yet revealing protocols. In particular, it would be most valuable to investigate the existence and the persistence of asymptotic residual shear strains, sustained after the shear stress is removed, at levels not only below the value at initial time but also above (as in section 3). So far we have identified only reports of experimental results concerned with elastomeric materials reinforced with *inextensible* fibers (and therefore with a ratio between the shear modulus of the bulk matrix and that of the fibers of several orders of magnitude), or concerned with moderate angles between the direction of shear and the fiber direction.

From a biomechanical point of view, the results have meaningful implications for biological soft tissues. First, the model captures adequately the elastic and the viscous anisotropies of biological materials (Baldwin et al. (2006), Taylor et al. (1990)). Second, although anomalous creep behaviors might preclude anomalous recovery behaviors, it is still useful to study the latter, because they might nonetheless arise in vivo following a stress-driven fiber orientation remodeling (Hariton et al. (2006)). Third, the effect of the prestretch on nonstandard behaviors is significant theoretically (section 4.3) as well as practically. (In vivo experiments show that large static prestretches of tendons reduce the risk of unexpected behaviors; see Kubo, Kanehisa, and Fukunaga (2002).) Finally, the results of the traveling wave study (section 5) may eventually lead to an acoustic (elastographic) determination of the fiber angle in soft tissues, through an efficient, simple, and noninvasive investigation.

Obviously, our results must be improved, and several directions are possible. Hence, two families of fibers have to be considered to give a better comparison with in vivo results for soft tissues. Also, the more realistic models of fiber reinforcements (such as the one proposed by Horgan and Saccomandi (2005) and by Gasser, Ogden, and Holzapfel (2006)) must be incorporated into the present study, to identify with a greater precision the range of parameters for which strange behaviors may occur.

Acknowledgment. G. S. thanks Gérard Maugin, Head of the Institut Jean Le Rond d'Alembert, for his hospitality.

REFERENCES

- S. L. BALDWIN, K. R. MARUTYAN, M. YANG, K. D. WALLACE, M. R. HOLLAND, AND J. G. MILLER (2006), *Measurements of the anisotropy of ultrasonic attenuation in freshly excised myocardium*, J. Acoust. Soc. Amer., 119, pp. 3130–3139.
- J. L. ERICKSEN (1953), *On the propagation of waves in isotropic incompressible perfectly elastic materials*, J. Ration. Mech. Anal., 2, pp. 329–337.
- Y. B. FU AND A. B. FREIDIN (2004), *Characterization and stability of two-phase piecewise-homogeneous deformations*, Proc. Royal Soc. Lond. A, 460, pp. 3065–3084.
- T. C. GASSER, R. W. OGDEN, AND G. A. HOLZAPFEL (2006), *Hyperelastic modelling of arterial layers with distributed collagen fibre orientations*, J. Roy. Soc. Interfaces, 3, pp. 15–25.
- N. GUNDIAH, M. B. RATCLIFFE, AND L. A. PRUITT (2007), *Determination of strain energy function for arterial elastin: Experiments using histology and mechanical tests*, J. Biomech., 40, pp. 586–594.
- I. HARITON, G. DEBOTTON, T. C. GASSER, AND G. A. HOLZAPFEL (2006), *Stress-driven collagen fiber remodeling in arterial walls*, TU Graz Online preprint reports, 68, pp. 1–26.
- G. A. HOLZAPFEL AND T. C. GASSER (2001), *A viscoelastic model for fiber-reinforced composites at finite strains: Continuum basis, computational aspects and applications*, Comput. Methods Appl. Mech. Engrg., 190, pp. 4379–4430.
- C. O. HORGAN AND G. SACCOMANDI (2005), *A new constitutive theory for fiber-reinforced incompressible nonlinearly elastic solids*, J. Mech. Phys. Solids, 53, pp. 1985–2025.

- J. D. HUMPHREY (2002), *Cardiovascular Solid Mechanics, Cells, Tissues and Organs*, Springer, New York.
- P. M. JORDAN AND A. PURI (2005), *A note on traveling wave solutions for a class of nonlinear viscoelastic media*, Phys. Lett. A, 335, pp. 150–156.
- K. KUBO, H. KANEHISA, AND T. FUKUNAGA (2002), *Effect of stretching training on the viscoelastic properties of human tendon structures in vivo*, J. Appl. Physiol., 92, pp. 595–601.
- Y. LIU, K. KASYANOV, AND R. T. SCHOEPHOERSTER (2007), *Effect of fiber orientation on the stress distribution within a leaflet of a polymer composite hearth valve in the closed position*, J. Biomech., 40, pp. 1099–1106.
- J. MERODIO AND R. W. OGDEN (2002), *Material instabilities in fiber-reinforced nonlinearly elastic solids under plane deformation*, Arch. Mech., 54, pp. 525–552.
- J. MERODIO AND R. W. OGDEN (2003), *Instabilities and loss of ellipticity in fiber-reinforced compressible non-linearly elastic solids under plane deformation*, Int. J. Solids Struct., 40, pp. 4707–4727.
- J. MERODIO AND R. W. OGDEN (2005a), *Mechanical response of fiber-reinforced incompressible nonlinear elastic solids*, Int. J. Nonlinear Mech., 40, pp. 213–227.
- J. MERODIO AND R. W. OGDEN (2005b), *On tensile instabilities and ellipticity loss in fiber-reinforced incompressible nonlinearly elastic solids*, Mech. Res. Comm., 32, pp. 290–299.
- J. MERODIO, G. SACCOMANDI, AND I. SGURA (2007), *The rectilinear shear of fiber-reinforced incompressible non-linearly elastic solids*, Int. J. Non-Linear Mech., 42, pp. 342–354.
- K. NISHIHARA (1995), *Stability of traveling waves with degenerate shock for systems of one-dimensional viscoelastic model*, J. Differential Equations, 120, pp. 304–318.
- G. J. PETTET, D. L. S. MCELWAIN, AND J. NORBURY (2000), *Lotka-Volterra equations with chemotaxis: Walls, barriers and travelling waves*, IMA J. Math. Control Inform., 17, pp. 395–413.
- G. Y. QIU AND T. J. PENCE (1997), *Remarks on the behavior of simple directionally reinforced incompressible nonlinearly elastic spheres*, J. Elasticity, 49, pp. 1–30.
- D. C. TAYLOR, J. D. DALTON, A. V. SEABER, AND W. E. GARRETT (1990), *Viscoelastic properties of muscle-tendon units. The biomechanical effects of stretching*, Amer. J. Sports Med., 18, pp. 300–309.
- N. TRIANTAFYLIDIS AND R. ABEYARATNE (1983), *Instabilities of a finitely deformed fiber-reinforced elastic material*, ASME J. Appl. Mech., 50, pp. 149–156.